ACS APPLIED POLYMER MATERIALS

pubs.acs.org/acsapm Article

Visualization of the pH Response through Autofluorescent Poly(styrene-*alt*-*N*-maleimide) Polyelectrolyte Brushes

Gozde Aktas Eken, Yuming Huang, Yixin Guo, and Christopher Ober*

Cite This: *ACS Appl. Polym. Mater.* 2023, 5, 1613−1623 Read Online

ACCESS | Metrics & More | Article Recommendations | Supporting Information

ABSTRACT: Polyelectrolyte brushes can undergo reversible conformational transitions in response to changes in environmental pH and ionic strength. Therefore, they offer great potential for the design of "smart" surfaces and surface-based sensing devices. Herein, we report weak acidic polyelectrolyte brushes with pH-dependent autofluorescence based on alternating copolymers of styrene and tailor-made *N*-maleimides, which exhibit "clusteroluminescence" due to the through-space conjugation of π-chromophoric subfluorophores. Swelling behavior of the polyelectrolyte brushes was evaluated as a function of pH via in-solution atomic force microscopy (AFM) analyses. The correlation between the pH-induced conformational transitions and autofluorescence was confirmed with confocal laser scanning microscopy (CLSM) and two-photon laser scanning microscopy. Poly(styrene-*alt*-*N*-maleimide)-based well-defined, stable polyelectrolyte brushes, generating optical signals from conformational changes without conventional fluorophores, may enable the design of sensors and optoelectronic devices.

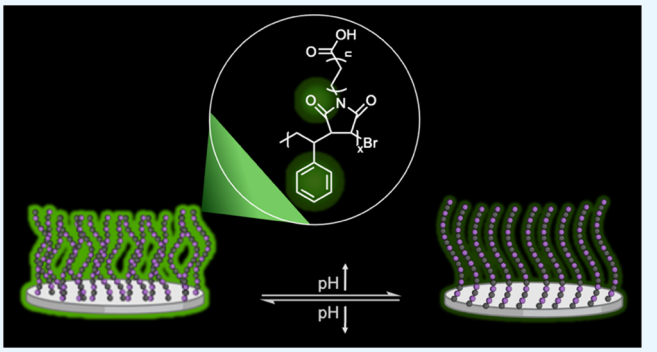

KEYWORDS: *polyelectrolyte brushes, autofluorescent brushes, alternating copolymers, smart surfaces, aggregation-induced emission*

INTRODUCTION

Polymer brushes enable the modification of surfaces over nm to μm length scales with precisely controlled end-functionality, composition, architecture, density, and thickness for a wide range of applications.[1−3] Conformations of polymer brushes can be dynamically modulated through external stimuli, which can lead to a transition from a fully extended chain to a collapsed state.[4] These reversible transitions between two states can be induced by changes in pH, ion content, temperature, solvent, and mechanical force and thus render them as suitable materials for the design of stimuli-responsive ("smart") surfaces.[5−7] Polyelectrolyte brushes (PEBs), which contain charged groups in their repeating units, have attracted considerable attention for the design of smart polymer interfaces, and many applications have been described for PEBs, including smart membranes,[8] enzyme immobilization supports,[9,10] smart actuators,[11] and responsive interfaces.[12] Specifically, weak polyelectrolyte brushes establish a versatile platform for responsive coatings since they can undergo dynamic changes in accordance with their degree of ionization and protonation, depending on the local pH.[13,14]

Polyelectrolyte brushes hold considerable potential for surface-based sensing materials, given the variety of functional and structural possibilities. However, these systems suffer from drawbacks, which are limiting their scope: stability and real-time analyses of conformational transitions. For example, degrafting of chains from the surface has been observed for both neutral and charged systems where the latter is subjected to additional forces in addition to the steric effects and osmotic pressure due to the electrostatic repulsion.[15,16] To date, two strategies have been commonly employed to enhance the stability of PEBs: (1) minimizing the number of labile bonds that may be susceptible to hydrolysis[17,18] and (2) introducing hydrophobic-neutral blocks between the substrate and charged segments to create a shielding layer and reduce the mechanical stresses at the polymer−substrate interface.[19,20] Recently, an effective approach was reported by our group, where alternating copolymerization was employed to dilute the charge density and thus reduce that tension.[21] We have designed strong cationic brushes via poly(styrene-*alt*-*N*-maleimide) copolymers, which facilitate the precise control of architecture, charge placement, and charge density.

Incorporation of luminescence into polymer brushes is a promising approach to overcome the limitations in real-time analysis of the conformational transitions and the dynamic

Received: December 23, 2022
Accepted: January 3, 2023
Published: January 18, 2023

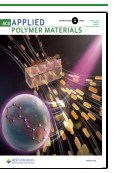

Scheme 1. Schematic Representation of (A) Synthesis of *N*-(*tert*-Butyl propanoate) Maleimide (MI_1), (B) Synthesis of *tert*-Butyl 3-(4-Hydroxybutoxy) Propanoate and *N*-(*tert*-Butyl(3-butoxy) propanoate) Maleimide (MI_2), and (C) Synthesis and Postsynthetic Modification of the Brushes (PMI_1 and PMI_2)

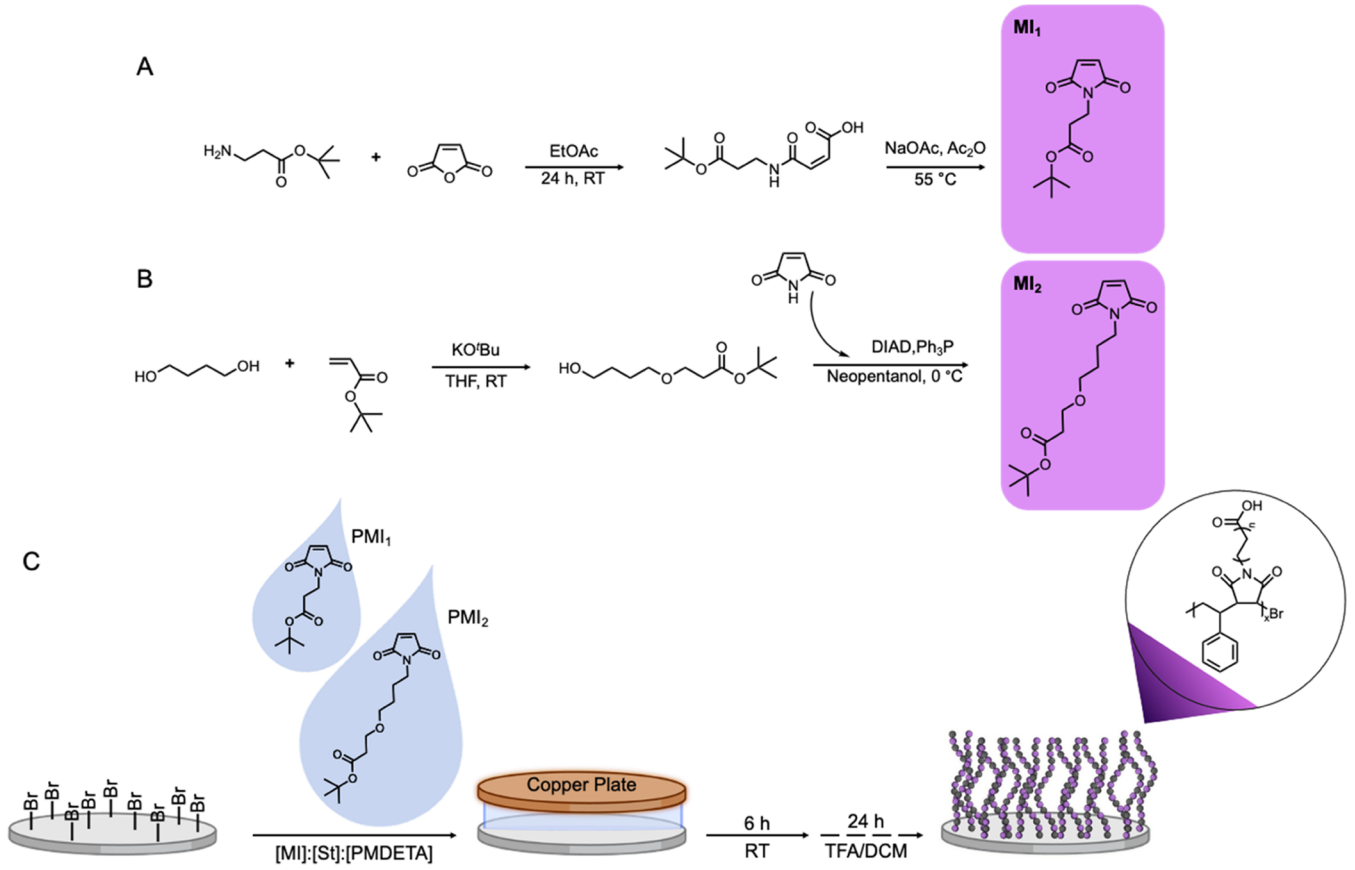

response of brushes to the environmental changes. Luminescent moieties can be introduced through copolymerization[22,23] using fluorophore-containing monomers or via postsynthetic modifications after brush growth, such as chain-end modifications.[24,25] However, there are several disadvantages of these approaches as most of the π-conjugated fluorophores have limited solubility in water. Incorporation of fluorophores into a polyelectrolyte brush structure can alter its intrinsic properties and cause chain collapse.[24,26] Precise placement and homogeneous distribution of fluorophore-containing monomers through copolymerization can be problematic due to different polymerization kinetics of comonomers. Fluorophore-containing monomers can also initiate photoinduced electron transfer reactions with the propagating radicals and lead to decreased polymerization rates.[27] Moreover, fluorophores within the closely packed brush structure can undergo self-quenching.

We suggest that these issues can be addressed by the use of autofluorescent polymers, which can emit fluorescence without the presence of conjugated polymeric building blocks and conventional fluorophores.[26,28] Autofluorescent behavior of poly(styrene-*alt*-*N*-maleimide) copolymers was reported recently,[29−31] which is associated with the "through-space" $\pi-\pi$ interactions of carbonyl groups of maleimides and the adjacent benzene ring of the styrene units.[26,32,33] Poly(styrene-*alt*-*N*-maleimide) copolymers are classified as luminogens with aggregation-induced emission effects (AIEgens), which generate clusters and luminesce strongly in the aggregated state. Using these AIEgens for the synthesis of stimuli-responsive polymer brushes may confer advanced functionalities to brush systems through visualization of conformational changes in addition to stability.[28,34]

Herein, we report well-defined weak acidic PEBs with pH-dependent luminescence for potential surface-based sensing devices. PEBs were prepared based on alternating copolymers of *N*-substituted maleimides and styrene through tailor-made maleimides to dilute charge density and adjust the distance between the charged groups and the backbone, which played an important role in stability and swelling properties. pH-dependent conformational changes from collapsed (~100 nm) to fully extended state conformations (~400 nm) altered the fluorescence characteristics, which were monitored via comparisons between in-solution AFM analyses and confocal laser scanning microscopy (CLSM). We showed that alternating copolymers of *N*-substituted maleimides and styrene enable the incorporation of sensing functionality in brush-integrated surfaces, which overcome the limitations of conventional fluorophores and low stability.

RESULTS AND DISCUSSION

Synthesis of *N*-substituted Maleimides and PEBs. *N*-substituted maleimides were synthesized with two different side chains, which enabled adjustment of the proximity of the ionic groups to the backbone. β-Alanine *t*-butyl ester has two methylene groups separating acidic units from the backbone, while *tert*-butyl 3-(4-hydroxybutoxy) propanoate contains six methylene groups between the acidic unit and the polymer

https://doi.org/10.1021/acsapm.2c02066
ACS Appl. Polym. Mater. 2023, 5, 1613−1623

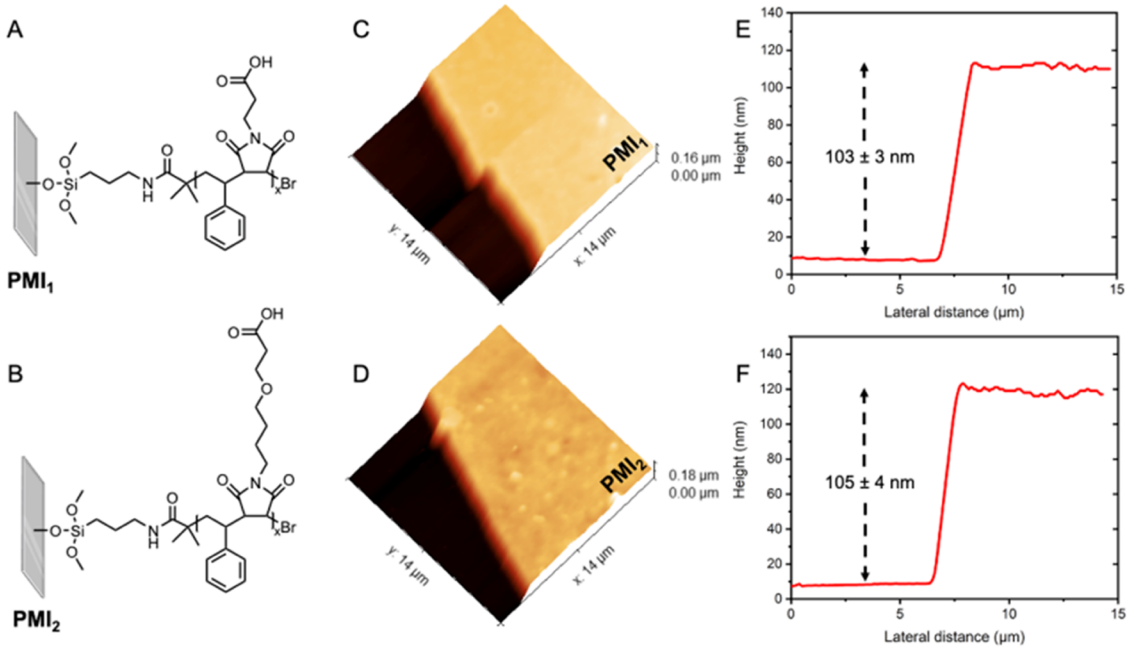

Figure 1. Chemical structure of the brushes (A) PMI_1 and (B) PMI_2. 3D height images of the brushes with scratched regions used for step-height measurements. (C) PMI_1 and (D) PMI_2. AFM height profiles exhibit the step-height difference between the bare wafer and the brush layer after hydrolysis of *tert*-butyl groups: (E) PMI_1 and (F) PMI_2.

backbone. *N*-substituted maleimides were synthesized via different methodologies (Scheme 1): *N*-(*tert*-butyl propanoate) maleimide (MI_1) was synthesized through the reaction of maleic anhydride with *β*-alanine *t*-butyl ester leading to a maleamic acid intermediate, which was subsequently dehydrated into maleimide. For the synthesis of *N*-(*tert*-butyl(3-butoxy) propanoate) maleimide (MI_2), a modified Mitsunobu method was employed, where *tert*-butyl 3-(4-hydroxybutoxy) propanoate was reacted with maleimide in the presence of triphenyl phosphine and a dialkyl azodicarboxylate. The successful synthesis of the products was confirmed with ^{1}H NMR (Figures S1−S4).

PEBs were grown from a surface-immobilized ATRP initiator (APTES-BIBB) through surface-initiated Cu(0)-mediated controlled radical polymerization, which enables the synthesis of thick, dense brush layers with low volumes of polymerization solutions and simple experimental setup at room temperature.[35,36] Polymerization solution was filled between an initiator-immobilized wafer and a copper plate, and then brush growth was determined at room temperature (25 °C) for 6 h. Brush thickness increased linearly with the polymerization time up to 6 h and leveled around 151 and 137 nm for brush series PMI_1 and PMI_2, respectively (Figure S5). Dry thickness of the resulting brushes was determined via AFM step-height measurements before and after hydrolysis of *tert*-butyl groups, where a noticeable decrease was observed upon the removal of bulky *t*-butyl groups due to relaxation (Figure 1E,F).

The composition of the poly(styrene-*alt*-*N*-maleimide) brushes was investigated via survey and high-resolution XPS scans. A representative survey spectrum of PMI_2 is presented in Figure 2A. In a perfectly alternating sequence, PMI_2 brushes are expected to contain 76% of C, 4% of N, and 20% of O. The surface composition determined via XPS survey analysis indicated that the copolymers exhibit alternating sequence with uniform distribution of maleimide and styrene units. High-resolution C 1s spectra of PMI_1 and PMI_2 are provided in Figure 2B,C. The C 1s spectrum of PMI_1 can be fitted with three curves with expected ratios, corresponding to C═C (286.9 eV), C−C (287.6 eV), and N−C═O/O−C═O (290.6 eV). The high-resolution signal of the PMI_2 requires an additional component, C−O−C (288.6 eV), due to the ether moiety in its side chain. To determine the precise composition of the copolymers, which is critical for the brush performance and stability, free copolymers of styrene and *N*-substituted maleimides were also synthesized and analyzed via ^{1}H NMR (Figures S6 and S7). The maleimide/styrene ratio was determined to be 45/55 and 43/57 for series PMI_1 and PMI_2, respectively.

As a complementary technique to XPS, near-edge X-ray absorption fine-structure spectroscopy (NEXAFS) was used to determine the near-surface composition and detailed chemical structure of the brushes. Figure 2D,E shows the postedge normalized C 1s NEXAFS spectra of brush surfaces acquired at an X-ray incidence angle of 55°. Similar NEXAFS spectra were obtained for PMI_1 and PMI_2. The first three sharp peaks at 284.9, 287.8, and 288.4 eV are assigned to C 1s $\pi^*_{C=C}$, C 1s σ^*_{C-H}, and C 1s $\pi^*_{C=O}$ transitions, respectively.[37,38] Since styrene units are the only source of aromatic structures, C 1s $\pi^*_{C=C}$ resonance is an indicator of the surface concentration of the hydrophobic segments, whereas the additional fine structures at 287.8 and 288.4 eV are indicative of maleimide segments populating the surface. The peak representing C 1s σ^*_{C-H} resonance has a greater intensity in PMI_2 than in PMI_1, which is consistent with the long aliphatic side chains. C 1s $\pi^*_{C=O}$ transitions may also include some contribution from the C 1s σ^*_{C-O} resonance due to etheric moieties in the side chain of PMI_2.[39] The broad peaks at higher energies at 293.5 and 303 eV are transitions to the σ^* orbitals and assigned to σ^*_{C-C}, σ^*_{C-N} and $\sigma^*_{C=C}$, $\sigma^*_{C=O}$, respectively.

https://doi.org/10.1021/acsapm.2c02066
ACS Appl. Polym. Mater. 2023, 5, 1613−1623

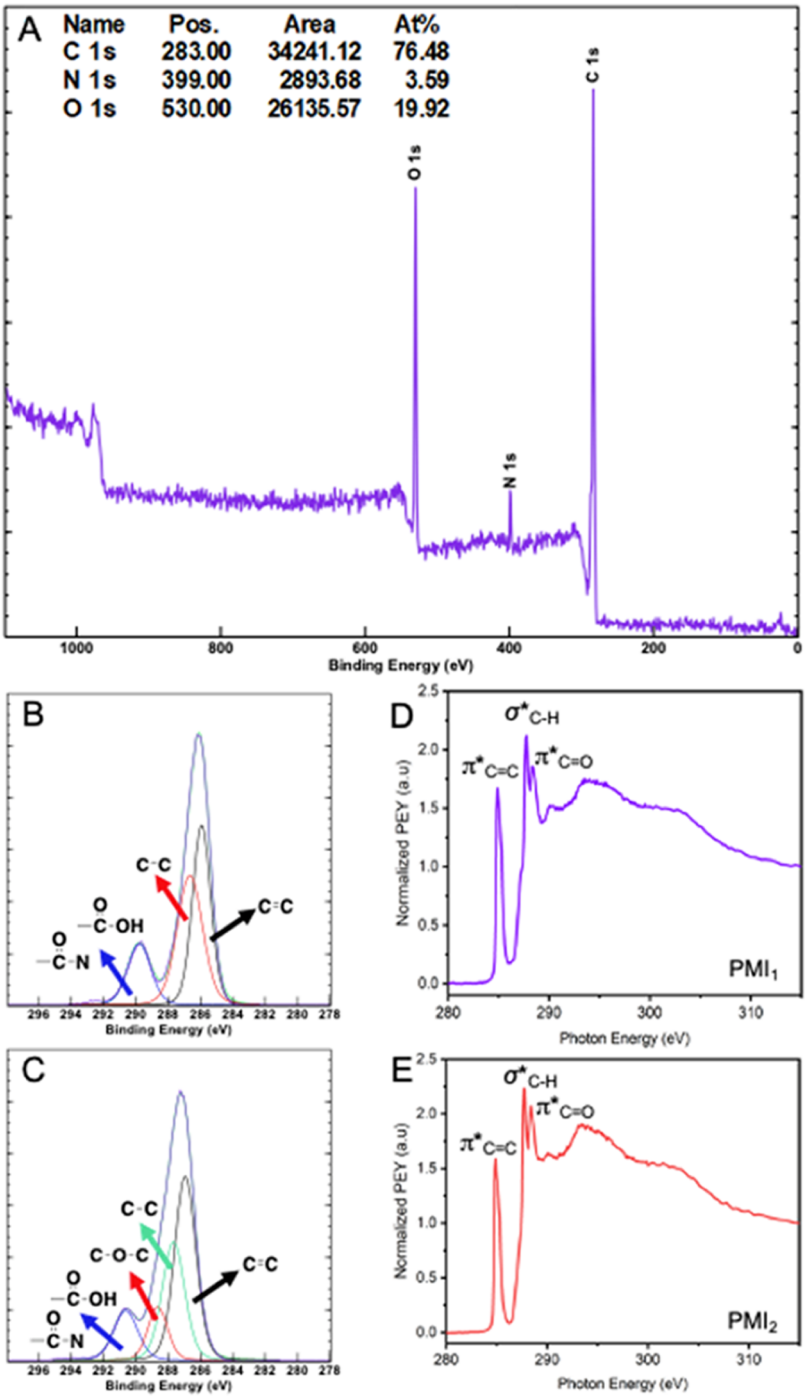

Figure 2. (A) XPS survey spectrum of PMI_2. (B) High-resolution C 1s spectrum of PMI_1. (C) High-resolution C 1s spectrum of PMI_2. C 1s NEXAFS spectra of the brush surfaces (D) PMI_1 and (E) PMI_2 obtained at an X-ray incidence angle of 55° and an entrance grid bias of −150 V.

pH-responsive swelling behavior of the brushes was investigated via in-solution AFM analyses. The samples were incubated in aqueous buffer solutions for 2 h and then analyzed in tapping mode. Since both PEBs have identical backbones, their swelling behaviors were expected to be defined by the side-chain composition (Figure S8). AFM data revealed that the steric effects are suppressed by the hydrophobic interactions, where PMI_1 with β-alanine-based shorter side chains displayed a higher swelling ratio at a given pH value. In the neutral state, these brushes had weak interactions with water, and thus brush thicknesses remained almost constant between pH 3 and 5. As the pH increased from 5 to 6, the thickness of poly(styrene-*alt*-*N*-maleimide) brushes sharply increased due to the deprotonation of acidic moieties, followed by a gradual increase with a further increase in pH up to 11. Figure 3A,B shows the swelling ratios of samples as a function of pH, which varied between 3.2 and 4.5 for PMI_1 and 2.2 and 3.3 for PMI_2. Representative height profiles are provided in Figures S9 and S10. Poly(styrene-*alt*-*N*-maleimide) brushes displayed similar morphologies during the transition from a collapsed to a fully extended state. When the brushes are in the neutral state, aqueous buffers (pH < 6) are poor solvents for both segments; therefore, polymer−polymer interactions become more favorable. After an

https://doi.org/10.1021/acsapm.2c02066
ACS Appl. Polym. Mater. 2023, 5, 1613−1623

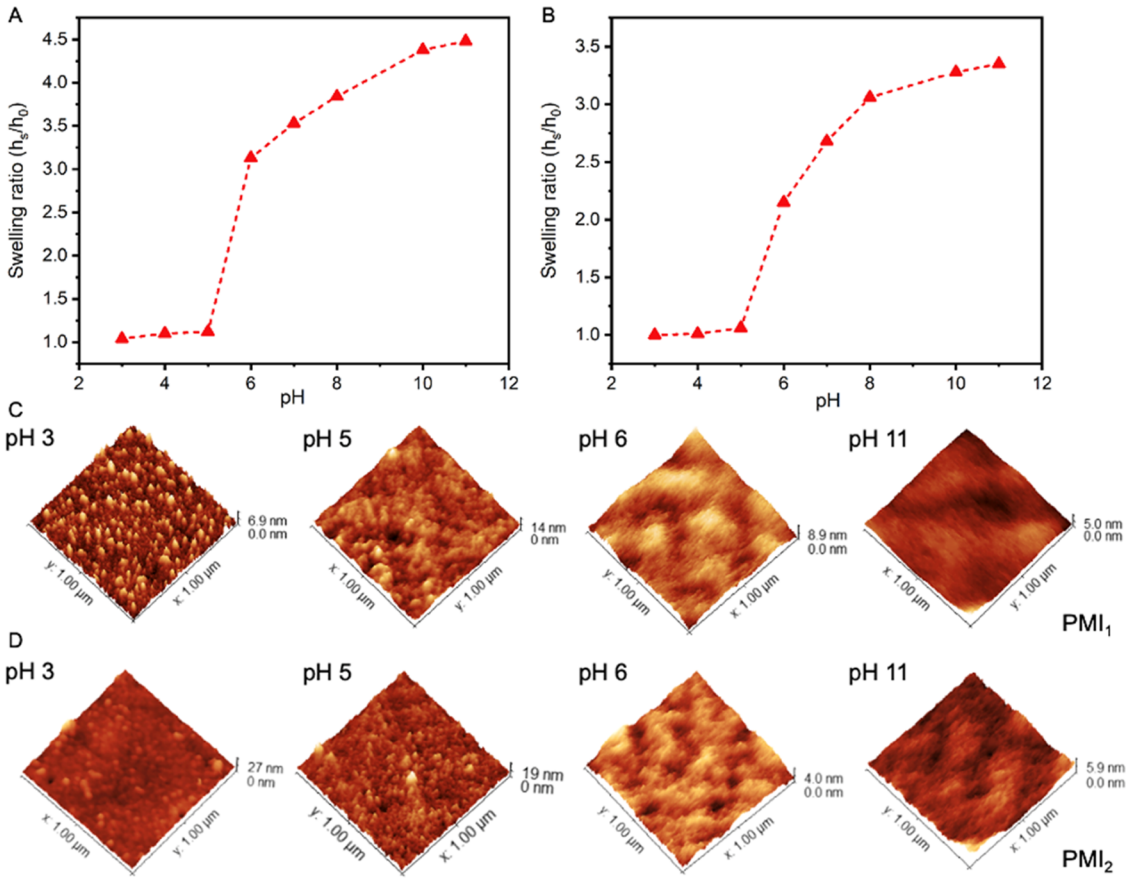

Figure 3. Swelling ratios of (A) PMI_1 and (B) PMI_2 in buffer solutions with various pHs. 3D AFM height images of the brushes after 2 h of incubation: (C) PMI_1 and (D) PMI_2.

incubation period, heterogenous features appeared on the top layer as a result of aggregated chains (Figure 3C,D). High contrast in the corresponding phase images also confirmed the formation of the aggregates (Figure S11). At pH 6 and above where acidic groups start to deprotonate, chains stretched away from the surface and created a homogeneous top layer. In the swollen state, brushes displayed homogeneous surfaces with relatively uniform phase behavior, and the swelling was accompanied by a significant reduction in RMS roughness (<1 nm).

Poly(styrene-*alt*-*N*-maleimide) copolymers are classified as aggregation-induced emission luminogens, and their photoluminescence behavior is associated with "through-space" $\pi-\pi$ interactions between the carbonyl and phenyl groups, which is induced by clusterization.[40] The theoretical and experimental analysis confirmed that the emissive behavior depends on the proximity and abundance of the subfluorophores and can be enhanced by increasing the amount of AIEgens.[28,41] The photophysical properties of free copolymers (deprotected) were analyzed under various conditions; first, we prepared solutions of copolymers (in THF) with various concentrations and measured fluorescence intensity as a function of concentration. The data confirmed the aggregation-induced emission behavior of copolymers where the fluorescence intensity increased with the increasing copolymer concentration (Figure 4A,B). For both copolymers, broad emission spectra were obtained (λ_{ex} = 400 nm) with an emission maximum around 485 nm (Figure 4C,D).

Next, the influence of pH on fluorescence intensity was examined. Since copolymers bear carboxylic acid groups in the side chains of maleimide units, it was anticipated that the degree of ionization would affect the chain conformation upon deprotonation and hence the clusteroluminescence. Therefore, deprotected copolymers were dissolved in buffer solutions (pH 7 and 11) (3 mg/mL), and fluorescence spectra were recorded. In alkaline solution, the extent of packing between the styrene and maleimide units is expected to decrease as a result of electrostatic repulsion along the polymeric backbone, which limits the $\pi-\pi$ interactions to some extent and results in lower emission intensity. The emission maximum was red-shifted to 526 nm for PMI_1 and to 532 nm for PMI_2, indicating a decrease in the emission energy due to the transition between the tautomers.[42] The copolymers exhibited stronger emission at pH 7, and a significant reduction was observed at pH 11. The latter condition corresponds to an extended chain conformation, leading to limited intra-/interchain interactions.[43]

pH-dependent clusteroluminescence of the PEBs was first qualitatively examined via CLSM, and z-stack images of the samples were recorded in acidic and basic environments to construct 3D images from the optical sections. Both samples exhibited greater fluorescence intensity in the collapsed state (pH 3) (Figure 5B,E), which drastically decreased upon swelling at pH 11 as a result of the reduced local density of polymer chains in the extended conformation (Figure 5C,F). The relationship between fluorescence intensity and brush conformation was quantitatively evaluated by two-photon laser

https://doi.org/10.1021/acsapm.2c02066
ACS Appl. Polym. Mater. 2023, 5, 1613−1623

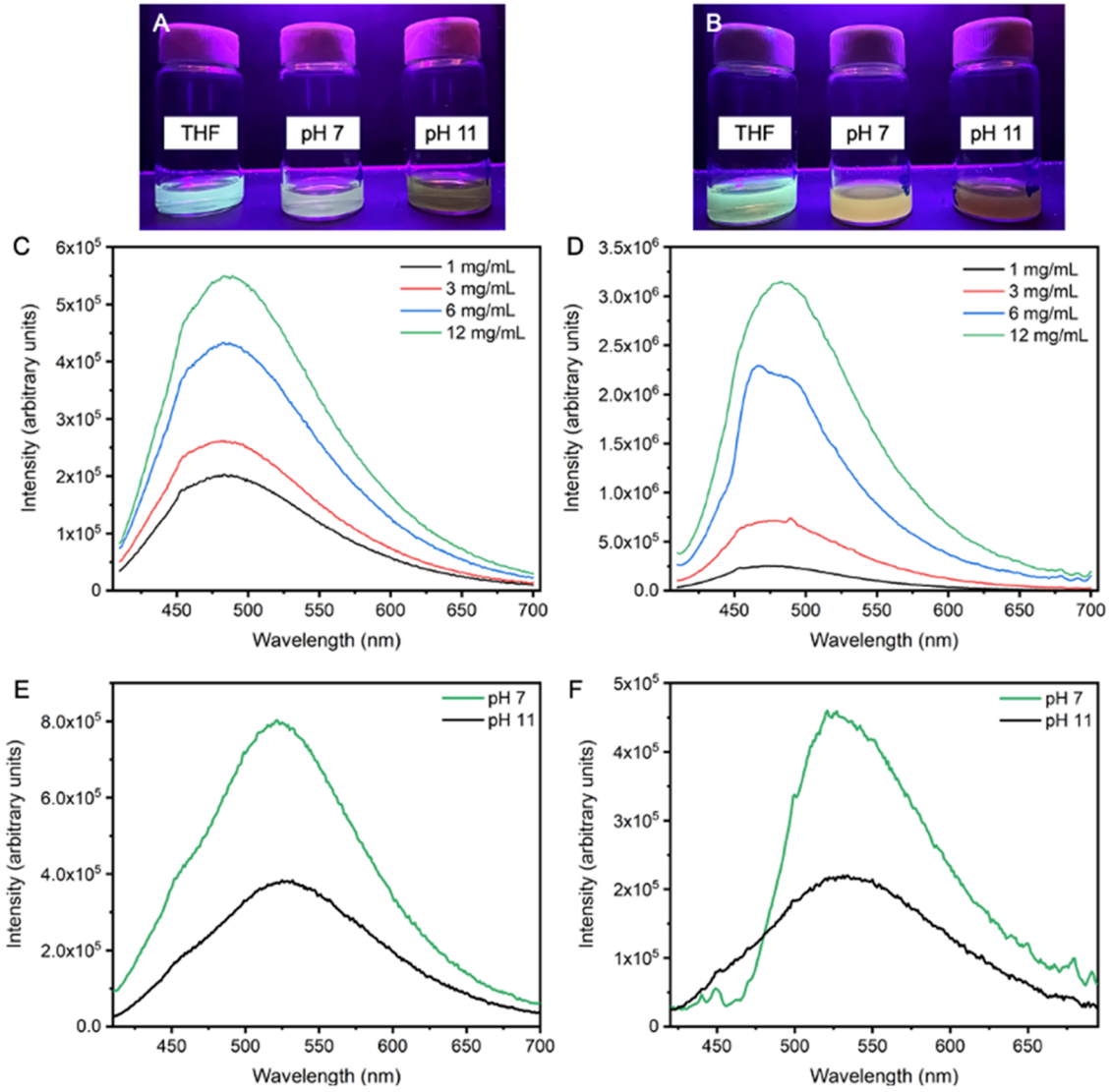

Figure 4. Digital photographs of solutions containing free deprotected copolymers dissolved in either THF or aqueous buffer solutions under UV light (3 mg/mL): (A) PMI_1 and (B) PMI_2. Fluorescence emission spectra of copolymers at different concentrations in THF: (C) PMI_1 and (D) PMI_2. Fluorescence emission spectra of deprotected polymers in aqueous buffer solutions (3 mg/mL): (E) PMI_1 and (F) PMI_2. All measurements were performed at 25 °C with λ_{ex} = 400 nm.

scanning microscopy. Fluorescence images were scanned in λ mode from 413 to 693 nm (λ_{ex} = 800 nm), in pHs 3, 6, 8, and 10, and the corresponding emission spectra were generated through 64 spectral sections (Figure 5D,G). Fluorescence spectra of the brushes correlated with that of free copolymers; however, the emission maximum shifted to a longer wavelength for PMI_1, indicating a decrease of the emission energy. Surfaces displayed a strong fluorescence signal at pH 3, where polymer chains were present in the collapsed state. In this form, polymer chains occupy smaller volumes compared to the swollen state, which leads to a higher local chain concentration. Such chain confinement facilitated space conjugation interactions and enhanced luminescence. The fluorescence intensity decreased as brushes switched from a collapsed to an extended state between pH 3 and 10. For PMI_2, a gradual decrease was observed in the fluorescence intensity, while the brush height slowly increased from 106 nm (pH 3) to 235 and 320 nm for pH 6 and 8, respectively. However, a steep decrease was observed for PMI_1 as a result of the sharp increase in the brush height from 108 nm (pH 3) to 333 and 383 nm for pH 6 and 8, respectively. In this state, adjacent chains are diluted with the hydration layer[44] and inter- and intramolecular interactions are limited by electrostatic repulsion as a result of increasing charge density. The results showed that the fluorescence intensity is defined by the conformational changes, which determines the local concentration of polymer chains and inter-/intramolecular interactions. Poly(styrene-*alt*-*N*-maleimide) brushes offer several advantages over conventional fluorophore-integrated systems, especially for those that require precise placement of molecules and often require additional postsynthetic modifications.

To investigate the effect of grafting density on clusteroluminescence of acidic poly(styrene-*alt*-*N*-maleimide) brushes, a brush sample prepared with styrene and MI_2 (h_0: 100 nm) was immersed in tetrabutyl ammonium fluoride (TBAF) solution to facilitate degrafting.[45] Grafting density was controlled with an incubation period in TBAF solution (1−3 h), and degrafting was confirmed with AFM analysis via the decrease of brush height. Then, the fluorescence intensity of the brushes was examined in the collapsed state (pH 3) as a

https://doi.org/10.1021/acsapm.2c02066
ACS Appl. Polym. Mater. 2023, 5, 1613−1623

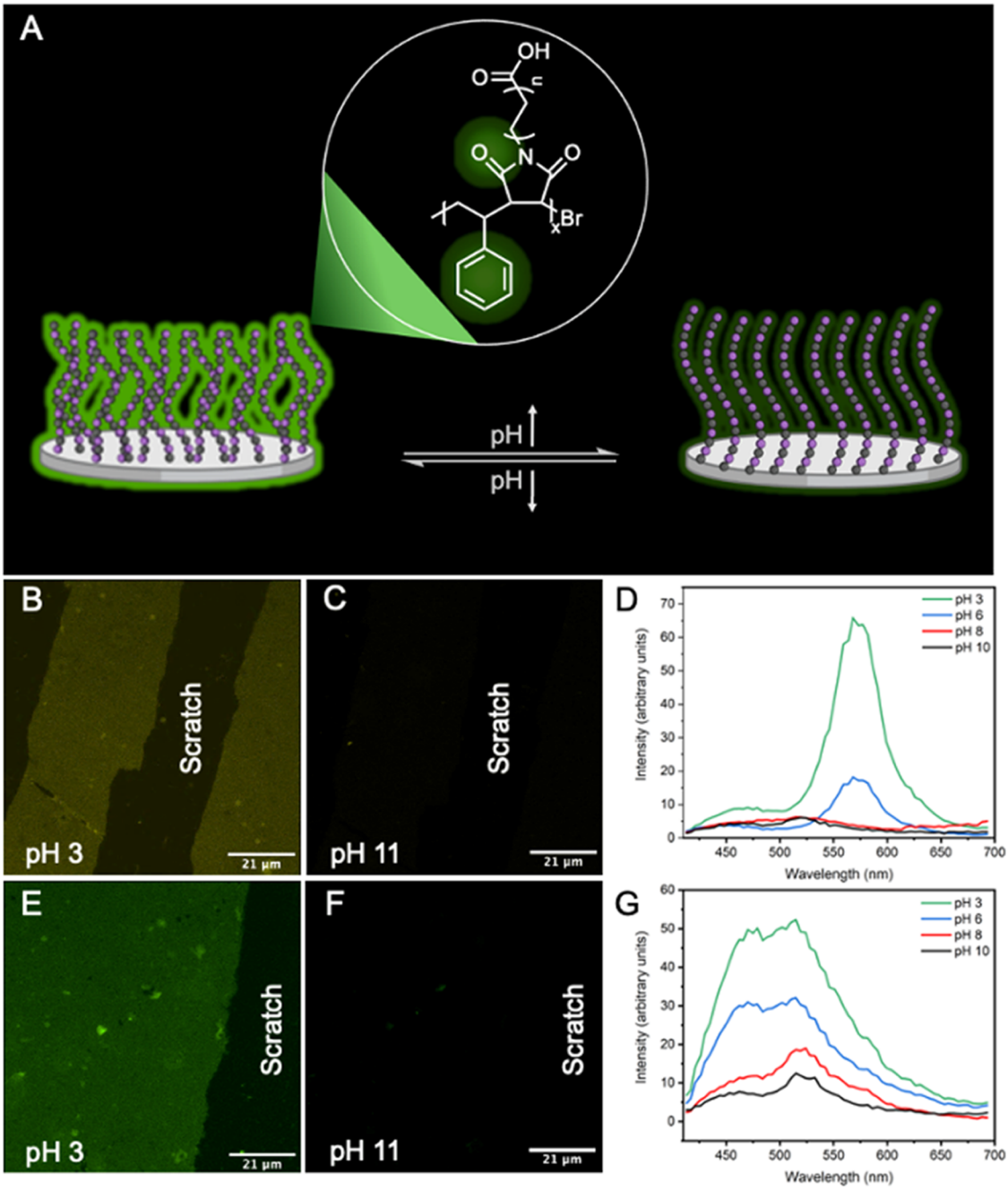

Figure 5. (A) Schematic representation of pH-triggered conformational change and luminescence of the brushes. CLSM images of the brushes: collapsed state (pH 3): (B) PMI_1 and (E) PMI_2; swollen state: (C) PMI_1 and (F) PMI_2 (pH 11). Fluorescence emission spectra of the polymer brush surfaces in buffer solutions with varying pHs, collected via two-photon excitation microscopy with λ_{ex} = 800 nm: (D) PMI_1 and (G) PMI_2.

function of grafting density. The fluorescence intensity gradually decreased with increasing incubation time, as a result of reduced local concentration of polymer chains and relatively relaxed conformation of the chains, limiting interactions between proximate subfluorophoric groups and cluster formation (Figure S12).

Brush systems that can generate optical signals from conformational changes without conventional fluorophores offer considerable potential for surface-based sensing devices:[30] (I) Autofluorescent polymers, which can be chemically attached to a substrate, enable to design reusable and stable sensors with enhanced photostability.[46,47] (II) Critical parameters such as water solubility, brush thickness, and distribution of the functional units can be precisely controlled to optimize the optical properties and amplification of sensor response.[40] (III) The rich chemistry of the substitution groups on monomers offers various combinations of the active sites for different applications. However, this functionality needs to be combined with stability to promote the applications of PEBs. To examine their stability and the role of alternating sequence and charge placement, brushes were incubated in aqueous buffer solutions for 12 days. Anionic brushes were incubated at pH 11 to mimic extreme conditions in which they are present in the charged state, which increases electrostatic repulsion and accelerates degrafting combined with base-catalyzed hydrolysis at a high concentration of the hydroxide ions.[18,48] To provide a

https://doi.org/10.1021/acsapm.2c02066
ACS Appl. Polym. Mater. 2023, 5, 1613−1623

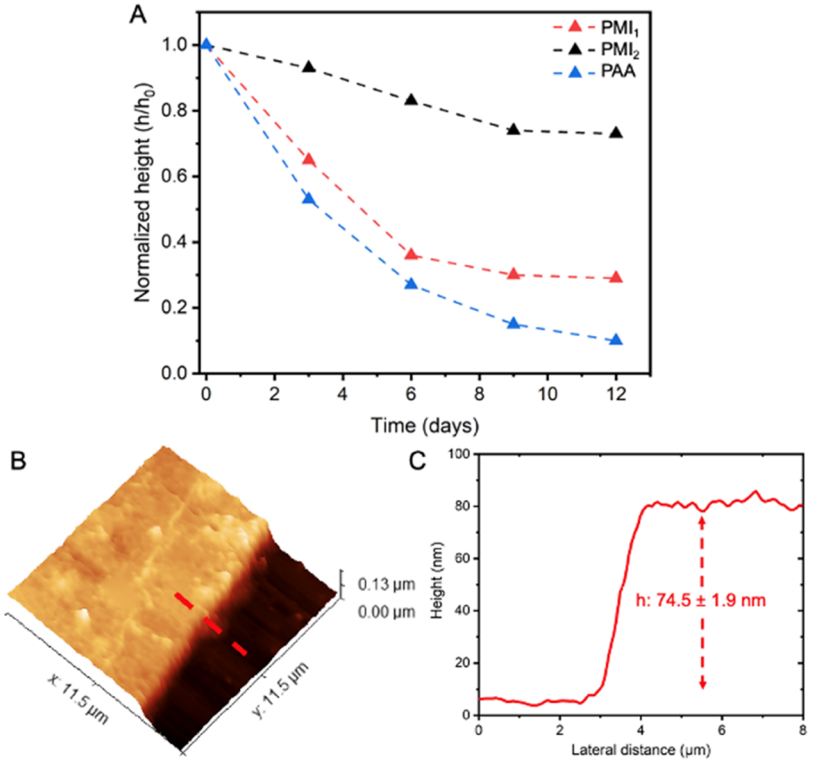

Figure 6. (A) Normalized dry thickness of the brushes measured after 12 days of incubation. (B) 3D height image of PMI_2 recorded after 11 weeks of incubation. (C) AFM height profile of PMI_2 after 11 weeks of incubation.

comparison with homopolymer-based systems, poly(acrylic acid) (PAA) brush (h_0: 83 nm), which is weak acidic polyelectrolytes with an acrylate-based backbone, is synthesized and evaluated under identical conditions. The samples were removed from the solution at certain time intervals, rinsed with DIW, and dried under vacuum, and then the dry brush thickness was measured via AFM. Figure 6A shows the normalized thickness of PMI_1, PMI_2, and PAA brushes as a function of incubation time. After 12 days of incubation, a significant reduction was observed in the normalized thickness of the PAA brush, which retained only 12% of its initial height. PMI_1 (h_0:103 nm), which contains a β-alanine-based spacer between the charged groups and the backbone, preserved ~30% of its initial height. However, PMI_2 (h_0: 105 nm) with a longer spacer, exhibited higher stability over the same period and retained more than 70% of its initial height. Figure S13 shows optical images of the substrates before and after incubation; substrates with PAA and PMI_1 brushes exhibited evident deterioration after stability tests. To test the limits of its stability, PMI_2 was incubated for up to 11 weeks, and the normalized thickness remained stable during that incubation period (Figure 6B,C), indicating that in addition to the alternating sequence, the distance between the charged groups and the backbone also plays an important role in stabilty of polyelectrolyte brushes.

CONCLUSIONS

In summary, we report weak polyelectrolyte brushes with pH-dependent autofluorescence based on poly(styrene-*alt*-*N*-maleimide) copolymers exhibit clusteroluminescence due to space conjugation of π-chromophoric subfluorophores. It was found that fluorescence intensity can be effectively regulated via brush conformation, which determines the abundance and inter-/intramolecular interactions of carbonyl and phenyl groups. In the collapsed state where polymers occupy smaller volumes, brushes emit strong fluorescence as a result of high polymer concentration, facilitating interactions between proximate subfluorophoric groups and cluster formation. Fluorescence intensity decreases upon swelling due to reduced concentration of polymers and extended conformation. The conformation-regulated autofluorescence of brushes was verified via comparisons between CLSM and in-solution AFM analyses in buffer solutions with varying pH. These brushes enable the design of smart surfaces without the need for conventional fluorophores and offer great potential for sensing devices.

EXPERIMENTAL SECTION

Materials. Maleic anhydride, magnesium sulfate ($MgSO_4$), and sodium chloride (NaCl) were obtained from BTC. Acetone-d_6, chloroform-d ($CDCl_3$), *tert*-butyl acrylate, *N*,*N*,*N*′,*N*″,*N*″-pentamethyldiethylenetriamine (PMDETA), tetrahydrofuran (THF), 1,4-butanediol, potassium *tert*-butoxide (KO^tBu), neopentyl alcohol, maleimide, diisopropyl azodicarboxylate (DIAD), triphenyl phosphine (Ph_3P), ethyl acetate, sodium acetate (NaAc), acetic anhydride, ethyl-2-bromoisobutyrate (EBiB), copper(II) bromide ($CuBr_2$), tris[2-(dimethylamino)ethyl]amine (Me_6TREN), *N*,*N*-dimethylformamide (DMF), triethylamine, α-bromoisobutyryl bromide (BIBB), ethanol (EtOH), dichloromethane (DCM), (3-aminopropyl)-triethoxysilane (APTES), trifluoroacetic acid (TFA), and styrene (St) were purchased from Sigma-Aldrich. β-Alanine *tert*-butyl ester hydrochloride and L-ascorbic acid were obtained from Fisher Scientific. Styrene was passed through an inhibitor removal column (Aldrich) before polymerization; others were used as received. A RiOs 3 Water Purification System was used to obtain deionized water (DIW). Silicon wafers (boron-doped, (100) orientation) were purchased from Pure Wafer.

https://doi.org/10.1021/acsapm.2c02066
ACS Appl. Polym. Mater. 2023, 5, 1613−1623

Synthesis of *N*-Substituted Maleimides. *N*-(*tert*-Butyl propanoate) maleimide was synthesized via a reaction of maleic anhydride and *β*-alanine tert-butyl ester. First, *β*-alanine *tert*-butyl ester hydrochloride was purified to remove the salt, which was dissolved in aqueous sodium hydroxide solution, and then extracted from the aqueous phase with DCM. The organic phase was collected over 3 extractions, and then the product was obtained after filtration and evaporation of the DCM.

Equimolar amounts of maleic anhydride and *β*-alanine tert-butyl ester were reacted in ethyl acetate at room temperature for 24 h. The maleamic acid, which precipitated as a white powder, was recovered by vacuum filtration, washed with ethyl acetate, and then dried and used without purification. For cyclization, maleamic acid was mixed with 0.3 mol equiv of anhydrous sodium acetate and 5.5 mol equiv of acetic anhydride. Then, the mixture was heated to 55 °C, and the reaction was monitored via ^{1}H NMR. The products were collected after 24 h through precipitation in ice-cold DIW, where *N*-(*tert*-butyl propanoate) maleimide was obtained as light brown powder with 70% yield.

Synthesis of *N*-(*tert*-Butyl(3-butoxy) propanoate) Maleimide. *tert*-Butyl 3-(4-hydroxybutoxy) propanoate was synthesized according to a previous report,[49] through monoalkylation of butanediol with *tert*-butyl acrylate. *tert*-Butyl acrylate (105 mmol) dissolved in 100 mL of anhydrous THF was added to a solution of butanediol (0.30 mol) and potassium *tert*-butoxide (100 mg) in 50 mL of anhydrous THF. The reaction was performed at room temperature for 24 h and neutralized with 1 M HCl. The solvent was evaporated, and the oily residue was dissolved in 200 mL of brine solution and then extracted with ethyl acetate three times. The combined organic layers were washed with 90 mL of brine and dried over Mg_2SO_4. The solvent was removed in vacuum, and the product was purified via column chromatography.

tert-Butyl 3-(4-hydroxybutoxy) propanoate (11.3 mmol), neopentyl alcohol (5.20 mmol), and triphenyl phosphine (10.3 mmol) were dissolved in 150 mL of anhydrous THF and cooled to 0 °C. Then, fine powder of maleimide (10.3 mmol) and DIAD (10.3 mmol) were added to the solution, which was kept at 0 °C for 5 min. Then, the reaction was performed for 12 h at room temperature. The solvent was removed, and the product was purified via column chromatography. *N*-(*tert*-Butyl(3-butoxy) propanoate) maleimide was obtained as a yellow viscous oil with 65% yield.

Synthesis of PEBs. Substrates with a surface-immobilized ATRP initiator with an amide linker were prepared and characterized as described below. Silicon wafers were cut into 1.5 × 3 cm^2 pieces and sonicated in acetone for 10 min and then dried under a nitrogen flow. Then, the substrates were exposed to oxygen plasma for 45 min. After plasma treatment, they were immersed in a solution of APTES 4% (v/v) in ethanol for 1 h and dried under N_2 and then baked for 30 min at 120 °C. APTES-treated wafers were immersed in a solution of BIBB (3 mmol) and TEA (3 mmol) in 15 mL of DCM for 24 h in an inert atmosphere. Wafers were removed from the solution, washed, and then stored in a desiccator.

One milliliter of polymerization mixture containing, [1]:[1]:[0.01] [St]/[MI]/[PMDETA] in 20:1 (v/v) DMSO/DIW was filled between an initiator-immobilized silicon wafer and a copper plate, which were separated by a Teflon spacer with a distance of d = 0.5 mm. The setup was then covered with a petri dish and polymerization was conducted at room temperature for 6 h. After polymerization, the plates were separated, and the substrates were sonicated in DMSO for 5 min. The substrates were dried and then immersed in 50 vol % solution of TFA/DCM for the deprotection of carboxylic acid groups.

Synthesis of Poly(styrene-*co*-*N*-maleimide) Copolymers. Poly(styrene-*co*-*N*-maleimide) copolymers were synthesized via ARGET-ATRP to determine the precise composition of the copolymers. Polymerizations were carried out for 24 h with given conditions: [MI]/[St]/[EBiB]/[$CuBr_2$]/[Me6TREN]/[L-ascorbic acid] = 250:250:1:0.05:0.5:1.5 in DMSO at 110 °C. The copolymers were precipitated in DIW and dried under vacuum at 40 °C for 12 h.

Characterization. *NMR Spectroscopy.* ^{1}H NMR spectra of the building blocks, monomers, and free polymers were recorded on a Varian Inova 500 spectrometer operating at 500 MHz at room temperature.

Atomic Force Microscopy. AFM measurements were conducted using an Oxford Instruments Cypher ES atomic force microscope equipped with an environmental scanner. Silicon tips (Oxford Instruments) with a resonance frequency of 300 kHz and a spring constant of 26 N/m were used for the dry state, while the tips with a frequency of 70 kHz and a spring constant of 2 N/m were used for in-fluid analyses. The dry and wet thickness of brushes was measured through step-height measurements by AFM. To measure brush thickness, the samples were carefully scratched with a razor blade, and AFM height images were taken at the boundary between scratched and nonscratched regions. Imaging was conducted in tapping mode, and the thickness of each sample was measured in three different regions. To determine the swelling ratio, the samples were incubated in buffer solutions and DIW for 2 h to equilibrate, and then the wet thickness of swollen brushes was measured.

X-ray Photoelectron Spectroscopy (XPS). X-ray photoelectron spectroscopy (XPS) analyses were conducted using a Scienta Omicron ESCA 2SR XPS equipped with a monochromatic Al K*α* high-power X-ray source operating at a power of 150 W with an emission current of 12.5 mA. The base pressure in the spectrometer was around 10^{-8} mbar. Survey spectra (5 scans) were collected with a pass energy of 200 eV and a step size of 1 eV, and high-resolution (10 scans) ones were collected with a pass energy of 50 eV and a step size of 0.05 eV. Casa XPS software was used for data processing including fitting.

NEXAFS Spectroscopy. NEXAFS spectroscopy was performed at the National Synchrotron Light Source II (NSLS-II) beamline 7ID-1 (SST-1) of Brookhaven National Lab. The samples were prepared on silicon wafers. The data reported were acquired using a grid bias of −150 V. The negative grid potential prevents electrons with kinetic energy less than 150 eV from entering the detector. The PEY signals were normalized by the incidence beam intensity obtained from the photo yield of a clean gold grid. A linear pre-edge baseline was subtracted from the normalized spectra, and the edge jump was arbitrarily set to unity far above the C K-edge.[50]

Contact Angle. Water contact angle (WCA) measurements were performed with an Attension Theta Lite goniometer using the sessile drop method; data were collected for a 10 s period within 60 s. The average of results was obtained from repeating measurements.

Fluorescence Measurements. Fluorescence emission spectra were recorded using the Edinburgh FLS 1000 Spectrometer (λ_{exc} = 370 nm, dλ = 1 nm, 380−700 nm) at RT in THF and buffer solutions (3 mg/mL).

Confocal Laser Scanning Microscopy (CLSM). Fluorescence imaging of polymer brushes was performed with a confocal microscope with an inverted Axio Observer Z.1 (ZEISS LSM710). A few drops of buffer solution were added between the cover glass and the substrate, then the samples were excited with an argon laser (405 nm), and emission was collected through 63× objective. Images were recorded with a constant set of parameters for all samples. The two-photon excited fluorescence spectra were collected using a Zeiss LSM 880 with an excitation wavelength of 800 nm and power of 10% using a 32× water immersion objective.

■ ASSOCIATED CONTENT

Supporting Information

The Supporting Information is available free of charge at https://pubs.acs.org/doi/10.1021/acsapm.2c02066.

^{1}H NMR spectra of building blocks, monomers, and polymers, AFM height profiles and phase images of swollen brushes, water contact angle of hydrolyzed brushes, and images of substrates before and after a stability test. (PDF)

https://doi.org/10.1021/acsapm.2c02066
ACS Appl. Polym. Mater. 2023, 5, 1613−1623

AUTHOR INFORMATION

Corresponding Author

Christopher Ober − *Materials Science and Engineering, Cornell University, Ithaca, New York 14853, United States;* orcid.org/0000-0002-3805-3314; Email: cko3@cornell.edu

Authors

Gozde Aktas Eken − *Materials Science and Engineering, Cornell University, Ithaca, New York 14853, United States;* orcid.org/0000-0002-4880-4089

Yuming Huang − *Materials Science and Engineering, Cornell University, Ithaca, New York 14853, United States;* orcid.org/0000-0002-1617-8570

Yixin Guo − *Materials Science and Engineering, Cornell University, Ithaca, New York 14853, United States;* orcid.org/0000-0002-2761-4972

Complete contact information is available at: https://pubs.acs.org/10.1021/acsapm.2c02066

Author Contributions

The manuscript was written through contributions of all authors. All authors have given approval to the final version of the manuscript.

Notes

The authors declare no competing financial interest.

ACKNOWLEDGMENTS

This study was primarily supported by the National Science Foundation through grant NSF CHE 200358. The authors would also like to acknowledge the Center for Research on Programmable Plant System (CROPPS) for the financial support with major support from the National Science Foundation under Grant No. DBI 2019674. This work made use of the Cornell Center for Materials Research Shared Facilities, which is supported through the NSF MRSEC program (DMR-1719875) and CESI Shared Facilities partly sponsored by the NSF MRI DMR-1338010 and Kavli Institute at Cornell (KIC). This work made use of the Cornell NMR Facility, which was supported, in part, by the NSF through MRI award CHE-1531632. This research used 7-ID Spectroscopy Soft and Tender (SST-1) beamline of the National Synchrotron Light Source II, a U.S. Department of Energy (DOE) Office of Science User Facility operated for the DOE Office of Science by Brookhaven National Laboratory under Contract No. DE-SC0012704. The authors thank Dr. C. Jaye, Dr. R. Medhi, and Dr. Z. Zhang for assisting with the experiments.

REFERENCES

(1) Chen, W.-L.; Cordero, R.; Tran, H.; Ober, C. K. 50th Anniversary Perspective: Polymer Brushes: Novel Surfaces for Future Materials. *Macromolecules* **2017**, *50*, 4089−4113.

(2) Zoppe, J. O.; Ataman, N. C.; Mocny, P.; Wang, J.; Moraes, J.; Klok, H.-A. Surface-Initiated Controlled Radical Polymerization: State-of-the-Art, Opportunities, and Challenges in Surface and Interface Engineering with Polymer Brushes. *Chem. Rev.* **2017**, *117*, 1105−1318.

(3) Feng, C.; Huang, X. Polymer Brushes: Efficient Synthesis and Applications. *Acc. Chem. Res.* **2018**, *51*, 2314−2323.

(4) Ma, S.; Zhang, X.; Yu, B.; Zhou, F. Brushing up functional materials. *NPG Asia Mater.* **2019**, *11*, 24.

(5) Li, D.; Xu, L.; Wang, J.; Gautrot, J. E. Responsive Polymer Brush Design and Emerging Applications for Nanotheranostics. *Adv. Healthcare Mater.* **2021**, *10*, No. 2000953.

(6) van Eck, G. C. R.; Chiappisi, L.; de Beer, S. Fundamentals and Applications of Polymer Brushes in Air. *ACS Appl. Polym. Mater.* **2022**, *4*, 3062−3087.

(7) Stuart, M. A. C.; Huck, W. T. S.; Genzer, J.; Müller, M.; Ober, C.; Stamm, M.; Sukhorukov, G. B.; Szleifer, I.; Tsukruk, V. V.; Urban, M.; Winnik, F.; Zauscher, S.; Luzinov, I.; Minko, S. Emerging applications of stimuli-responsive polymer materials. *Nat. Mater.* **2010**, *9*, 101−113.

(8) Khor, C. M.; Zhu, X.; Messina, M. S.; Poon, S.; Lew, X. Y.; Maynard, H. D.; Jassby, D. Electrically Mediated Membrane Pore Gating via Grafted Polymer Brushes. *ACS Mater. Lett.* **2019**, *1*, 647−654.

(9) Ferrand-Drake del Castillo, G.; Koenig, M.; Müller, M.; Eichhorn, K.-J.; Stamm, M.; Uhlmann, P.; Dahlin, A. Enzyme Immobilization in Polyelectrolyte Brushes: High Loading and Enhanced Activity Compared to Monolayers. *Langmuir* **2019**, *35*, 3479−3489.

(10) Yang, Q.; Li, L.; Sun, L.; Ye, Z.; Wang, Y.; Guo, X. Spherical polyelectrolyte brushes as bio-platforms to integrate platinum nanozyme and glucose oxidase for colorimetric detection of glucose. *J. Polym. Sci.* **2021**, *59*, 2201−2211.

(11) Li, B.; Du, T.; Yu, B.; van der Gucht, J.; Zhou, F. Caterpillar-Inspired Design and Fabrication of A Self-Walking Actuator with Anisotropy, Gradient, and Instant Response. *Small* **2015**, *11*, 3494−3501.

(12) Li, M.; Pester, C. W. Mixed Polymer Brushes for "Smart" Surfaces. *Polymers* **2020**, *12*, 1553.

(13) Geoghegan, M. Weak polyelectrolyte brushes. *Soft Matter* **2022**, *18*, 2500−2511.

(14) Schüwer, N.; Klok, H.-A. Tuning the pH Sensitivity of Poly(methacrylic acid) Brushes. *Langmuir* **2011**, *27*, 4789−4796.

(15) Tugulu, S.; Klok, H.-A. Stability and Nonfouling Properties of Poly(poly(ethylene glycol) methacrylate) Brushes under Cell Culture Conditions. *Biomacromolecules* **2008**, *9*, 906−912.

(16) Klok, H.-A.; Genzer, J. Expanding the Polymer Mechanochemistry Toolbox through Surface-Initiated Polymerization. *ACS Macro Lett.* **2015**, *4*, 636−639.

(17) Ataman, N. C.; Klok, H.-A. Degrafting of Poly(poly(ethylene glycol) methacrylate) Brushes from Planar and Spherical Silicon Substrates. *Macromolecules* **2016**, *49*, 9035−9047.

(18) Galvin, C. J.; Bain, E. D.; Henke, A.; Genzer, J. Instability of Surface-Grafted Weak Polyacid Brushes on Flat Substrates. *Macromolecules* **2015**, *48*, 5677−5687.

(19) Li, Y.; Ko, Y.; Lin, Y.; Kiserow, D.; Genzer, J. Enhanced Stability of Surface-Tethered Diblock Copolymer Brushes with a Neutral Polymer Block and a Weak Polyelectrolyte Block: Effects of Molecular Weight and Hydrophobicity of the Neutral Block. *Macromolecules* **2017**, *50*, 8580−8587.

(20) Quintana, R.; Gosa, M.; Jańczewski, D.; Kutnyanszky, E.; Vancso, G. J. Enhanced Stability of Low Fouling Zwitterionic Polymer Brushes in Seawater with Diblock Architecture. *Langmuir* **2013**, *29*, 10859−10867.

(21) Aktas Eken, G.; Ober, C. K. Strong Polyelectrolyte Brushes via Alternating Copolymers of Styrene and Maleimides: Synthesis, Properties, and Stability. *Macromolecules* **2022**, *55*, 5291−5300.

(22) Besford, Q. A.; Yong, H.; Merlitz, H.; Christofferson, A. J.; Sommer, J.-U.; Uhlmann, P.; Fery, A. FRET-Integrated Polymer Brushes for Spatially Resolved Sensing of Changes in Polymer Conformation. *Angew. Chem., Int. Ed.* **2021**, *60*, 16600−16606.

(23) Besford, Q. A.; Merlitz, H.; Schubotz, S.; Yong, H.; Chae, S.; Schnepf, M. J.; Weiss, A. C. G.; Auernhammer, G. K.; Sommer, J.-U.; Uhlmann, P.; Fery, A. Mechanofluorescent Polymer Brush Surfaces that Spatially Resolve Surface Solvation. *ACS Nano* **2022**, *16*, 3383−3393.

(24) Tas, S.; Kopec, M.; van der Pol, R.; Cirelli, M.; de Vries, I.; Bölükbas, D. A.; Tempelman, K.; Benes, N. E.; Hempenius, M. A.;

Vancso, G. J.; de Beer, S. Chain End-Functionalized Polymer Brushes with Switchable Fluorescence Response. *Macromol. Chem. Phys.* **2019**, *220*, No. 1800537.
(25) Dai, X.; Zhou, F.; Khan, N.; Huck, W. T. S.; Kaminski, C. F. Direct Visualization of Reversible Switching of Micropatterned Polyelectrolyte Brushes on Gold Surfaces Using Laser Scanning Confocal Microscopy. *Langmuir* **2008**, *24*, 13182−13185.
(26) Zhang, H.; Zhao, Z.; McGonigal, P. R.; Ye, R.; Liu, S.; Lam, J. W. Y.; Kwok, R. T. K.; Yuan, W. Z.; Xie, J.; Rogach, A. L.; Tang, B. Z. Clusterization-triggered emission: Uncommon luminescence from common materials. *Mater. Today* **2020**, *32*, 275−292.
(27) Spiniello, M.; Blencowe, A.; Qiao, G. G. Synthesis and characterization of fluorescently labeled core cross-linked star polymers. *J. Polym. Sci., Part A: Polym. Chem.* **2008**, *46*, 2422−2432.
(28) Chatterjee, D. P.; Pakhira, M.; Nandi, A. K. Fluorescence in "Nonfluorescent" Polymers. *ACS Omega* **2020**, *5*, 30747−30766.
(29) Saha, B.; Bauri, K.; Bag, A.; Ghorai, P. K.; De, P. Conventional fluorophore-free dual pH- and thermo-responsive luminescent alternating copolymer. *Polym. Chem.* **2016**, *7*, 6895−6900.
(30) Bauri, K.; Saha, B.; Mahanti, J.; De, P. A nonconjugated macromolecular luminogen for speedy, selective and sensitive detection of picric acid in water. *Polym. Chem.* **2017**, *8*, 7180−7187.
(31) Saha, B.; Choudhury, N.; Seal, S.; Ruidas, B.; De, P. Aromatic Nitrogen Mustard-Based Autofluorescent Amphiphilic Brush Copolymer as pH-Responsive Drug Delivery Vehicle. *Biomacromolecules* **2019**, *20*, 546−557.
(32) Yan, J.-J.; Wang, Z.-K.; Lin, X.-S.; Hong, C.-Y.; Liang, H.-J.; Pan, C.-Y.; You, Y.-Z. Polymerizing Nonfluorescent Monomers without Incorporating any Fluorescent Agent Produces Strong Fluorescent Polymers. *Adv. Mater.* **2012**, *24*, 5617−5624.
(33) Ru, Y.; Zhang, X.; Song, W.; Liu, Z.; Feng, H.; Wang, B.; Guo, M.; Wang, X.; Luo, C.; Yang, W.; Li, Y.; Qiao, J. A new family of thermoplastic photoluminescence polymers. *Polym. Chem.* **2016**, *7*, 6250−6256.
(34) Poisson, J.; Hudson, Z. M. Luminescent Surface-Tethered Polymer Brush Materials. *Chem. − Eur. J.* **2022**, *28*, No. e202200552.
(35) Zhang, T.; Du, Y.; Müller, F.; Amin, I.; Jordan, R. Surface-initiated Cu(0) mediated controlled radical polymerization (SI-CuCRP) using a copper plate. *Polym. Chem.* **2015**, *6*, 2726−2733.
(36) Zhang, T.; Du, Y.; Kalbacova, J.; Schubel, R.; Rodriguez, R. D.; Chen, T.; Zahn, D. R. T.; Jordan, R. Wafer-scale synthesis of defined polymer brushes under ambient conditions. *Polym. Chem.* **2015**, *6*, 8176−8183.
(37) Krishnan, S.; Paik, M. Y.; Ober, C. K.; Martinelli, E.; Galli, G.; Sohn, K. E.; Kramer, E. J.; Fischer, D. A. NEXAFS Depth Profiling of Surface Segregation in Block Copolymer Thin Films. *Macromolecules* **2010**, *43*, 4733−4743.
(38) Krishnan, S.; Ayothi, R.; Hexemer, A.; Finlay, J. A.; Sohn, K. E.; Perry, R.; Ober, C. K.; Kramer, E. J.; Callow, M. E.; Callow, J. A.; Fischer, D. A. Anti-Biofouling Properties of Comblike Block Copolymers with Amphiphilic Side Chains. *Langmuir* **2006**, *22*, 5075−5086.
(39) Dimitriou, M. D.; Zhou, Z.; Yoo, H.-S.; Killops, K. L.; Finlay, J. A.; Cone, G.; Sundaram, H. S.; Lynd, N. A.; Barteau, K. P.; Campos, L. M.; Fischer, D. A.; Callow, M. E.; Callow, J. A.; Ober, C. K.; Hawker, C. J.; Kramer, E. J. A General Approach to Controlling the Surface Composition of Poly(ethylene oxide)-Based Block Copolymers for Antifouling Coatings. *Langmuir* **2011**, *27*, 13762−13772.
(40) Bauri, K.; Saha, B.; Banerjee, A.; De, P. Recent advances in the development and applications of nonconventional luminescent polymers. *Polym. Chem.* **2020**, *11*, 7293−7315.
(41) Nishimori, K.; Ouchi, M. AB-alternating copolymers via chain-growth polymerization: synthesis, characterization, self-assembly, and functions. *Chem. Commun.* **2020**, *56*, 3473−3483.
(42) Ahn, H.; Hong, J.; Kim, S. Y.; Choi, I.; Park, M. J. A pH-Responsive Molecular Switch with Tricolor Luminescence. *ACS Appl. Mater. Interfaces* **2015**, *7*, 704−712.
(43) Kirwan, L. J.; Papastavrou, G.; Borkovec, M.; Behrens, S. H. Imaging the Coil-to-Globule Conformational Transition of a Weak Polyelectrolyte by Tuning the Polyelectrolyte Charge Density. *Nano Lett.* **2004**, *4*, 149−152.
(44) Yamazoe, K.; Higaki, Y.; Inutsuka, Y.; Miyawaki, J.; Cui, Y.-T.; Takahara, A.; Harada, Y. Enhancement of the Hydrogen-Bonding Network of Water Confined in a Polyelectrolyte Brush. *Langmuir* **2017**, *33*, 3954−3959.
(45) Patil, R. R.; Turgman-Cohen, S.; Šrogl, J.; Kiserow, D.; Genzer, J. Direct Measurement of Molecular Weight and Grafting Density by Controlled and Quantitative Degrafting of Surface-Anchored Poly(methyl methacrylate). *ACS Macro Lett.* **2015**, *4*, 251−254.
(46) Yan, J.-J.; Wang, X.-Y.; Wang, M.-Z.; Pan, D.-H.; Yang, R.-L.; Xu, Y.-P.; Wang, L.-Z.; Yang, M. Self-Assembling Nonconjugated Poly(amide-imide) into Thermoresponsive Nanovesicles with Unexpected Red Fluorescence for Bioimaging. *Biomacromolecules* **2019**, *20*, 1455−1463.
(47) Liu, B.; Wang, Y.-L.; Bai, W.; Xu, J.-T.; Xu, Z.-K.; Yang, K.; Yang, Y.-Z.; Zhang, X.-H.; Du, B.-Y. Fluorescent linear CO2-derived poly(hydroxyurethane) for cool white LED. *J. Mater. Chem. C* **2017**, *5*, 4892−4898.
(48) Borozenko, O.; Godin, R.; Lau, K. L.; Mah, W.; Cosa, G.; Skene, W. G.; Giasson, S. Monitoring in Real-Time the Degrafting of Covalently Attached Fluorescent Polymer Brushes Grafted to Silica Substrates—Effects of pH and Salt. *Macromolecules* **2011**, *44*, 8177−8184.
(49) Warnecke, A.; Kratz, F. Maleimide-oligo(ethylene glycol) Derivatives of Camptothecin as Albumin-Binding Prodrugs: Synthesis and Antitumor Efficacy. *Bioconjugate Chem.* **2003**, *14*, 377−387.
(50) Stöhr, J. Analysis of K-Shell Excitation Spectra by Curve Fitting. In *NEXAFS Spectroscopy*; Stöhr, J., Ed.; Springer: Berlin, 1992; pp 211−238.

https://doi.org/10.1021/acsapm.2c02066
ACS Appl. Polym. Mater. 2023, 5, 1613−1623